International Journal of Chemical and Biochemical Sciences
(ISSN 2226-9614)

Journal Home page: www.iscientific.org/Journal.html

Analysis of the Structural and Optical Properties of SnO_2 Nanoparticles Fabricated via Biosynthesis with *Pandanus Amaryllifolius*

Irmaizatussyehdany Buniyamin[1,3*], Kevin Alvin Eswar[1,3,4], Maryam Mohammad[1,3,5] Muhammad Salleh Shamsudin[6,7], Mohamad Rusop Mahmood[1,2], Zuraida Khusaimi[1,3*]

[1]NANO-SciTech Laboratory, Centre for Functional Materials and Nanotechnology (FMN), Institute of Science, Universiti Teknologi MARA (UiTM), 40450 Shah Alam Selangor, Malaysia
[2]NANO-ElecTronic Centre, Engineering College, Universiti Teknologi MARA (UiTM), 40450 Shah Alam Selangor, Malaysia
[3]Faculty of Applied Sciences, Universiti Teknologi MARA (UiTM), 40450 Shah Alam Selangor, Malaysia
[4]Faculty of Applied Sciences, Universiti Teknologi MARA (UiTM) Sabah Branch Tawau Campus, 91032 Tawau Sabah, Malaysia
[5]Faculty of Applied Sciences, Universiti Teknologi MARA (UiTM) Perak Branch Tapah Campus, 35000 Tapah Road Perak, Malaysia
[6]Smart Manufacturing and Systems Research Group (SMSRG), University of Southampton Malaysia (UoSM), 79100 Iskandar Puteri Johor, Malaysia
[7]School of Engineering, Faculty of Engineering and Physical Sciences, University of Southampton Malaysia (UoSM), 79100 Iskandar Puteri Johor, Malaysia

Abstract

Tin oxide nanoparticles (SnO_2 NPs) were synthesized employing a straightforward green-synthesis method via *Pandanus amaryllifolius* leaves extract. This method has proven to be an efficient alternative to replace the conventional method that is knowingly costly, hazardous, time-consuming, and utilizes high energy. The structural, morphological, and optical properties were studied using various thermal calcination temperatures. XRD analysis showed that the crystallite size increases as the temperature rises, and the lower dislocation density and lattice distortion value increases the crystallite size. FTIR obtained pertinent functional groups belonging to SnO_2 construction based on the Sn-O-Sn and Sn-OH absorption peaks, regardless of the temperature variation. The morphological evidence from FESEM analysis showed the presence of spherical nanoparticles with uniform distribution, with larger SnO_2 NPs produced at a higher temperature. In addition, EDX analysis confirmed the presence of Sn and O elements. The band gap obtained was between 4.75 eV to 4.90 eV as the temperature increased, thus suggesting that the absorption edge was in blue shifted, owing to the quantum confinement effect. By having this result, SnO_2 NPs are recommended to be utilized for water photocatalytic application specifically for remediation purposes.

Keywords: Tin oxide nanoparticles, *Pandanus amaryllifolius*, Biosynthesis, Structural, Optical

Full length article **Corresponding Author*, e-mail: *syehdany@uitm.edu.my, zurai142@uitm.edu.my*

1. Introduction

Nanomaterials have been classified as 1D materials, and the sizes are identified within 1 to 100 nm [1]. The very tinny size and high surface area-to-volume ratio appear state-of-the-art, bringing new enhancement in terms of characteristics and efficiency, especially in optical, magnetic, electrical, and catalytic activities [2]. The uniqueness of nanomaterials has allowed them to be applied in many technological applications in the fields of physic, chemistry, biomedicine and material sciences [3]. Recently, immense attention has been gained to tin (iv) oxide nanoparticles (SnO_2 NPs) as it displays a variety of novel attributes such as potential chemical properties, thermal strength, and biocompatibility [4]. These semiconductor materials own capabilities in performing beneficial applications such as lithium-ion batteries, optoelectronic devices, solar cells, electrodes, light-emitting diodes, gas sensors, coatings, catalysts, and biomedicals [5-14]. From the perspective of material technology, SnO_2 NPs is categorized as an oxygen-deficient n-type semiconductor with a band gap energy of 3.6 to 3.8 eV.

The crystallite tetragonal rutile structure of SnO_2 NPs has lattice constants of a = b = 4.7374 Å and c = 3.1864 Å [15]. For the record, SnO_2 NPs has a high melting point of about 1127 °C and an exciton binding energy of 1300 meV (at 293 K). Furthermore, SnO_2 NPs is known to possess great thermal stability, whereby it can reach up to 500°C, low electrical resistance and low density. Moreover, SnO_2 NPs is highly transparent in the visible spectrum and competent to have strong chemical and physical interactions with the adsorbent [16]. These distinctive physicochemical properties and potential application of SnO_2 NPs have stimulated researchers to develop several methods for their production. The method of production, which is known as the chemical and physical synthesis SnO_2 NPs is considered costly and employs toxic materials that are harmful to human health and the ecosystem such as hydrothermal, sol-gel, co-precipitation, microwave-assisted, laser ablation, and spray pyrolysis [17-22]. In the past few years, the research interest in the green synthesis of SnO_2 NPs has been gained owing to its many advantages: it offers simplicity, is environmental friendly, and is a sustainable, economical, and reproducible method [23]. To accomplish this purpose, non-toxic solvents and natural resources are necessary. The production of SnO_2 NPs via the green synthesis method employed a variety of plant extracts from different plant segments, in which the sizable output occurs in a more straightforward process. Various plant extracts have been broadly studied to facilitate the green synthesis of SnO_2 NPs, as described by Matussin and co-workers, in which numerous phytochemical compounds in the plant extracts; flavonoids, polyphenols, glucose, terpenoids, carboxylic acids, ketones, aldehydes, and amides, were found to mediate the reduction of metal salt into metal nanoparticles [24]. This article intends to characterize the nanocrystalline SnO_2 NPs synthesized by the green synthesis method using the leaves extract of *Pandanus Amaryllifolius* (*P. amaryllifolius*). *P. amaryllifolius* leaves is a local plant in Malaysia that have been traditionally used as food and beverage flavoring, which contain useful phytochemical as the reducing agent, the flavonoid compound [25-26]. In the present work, we have investigated various characteristics of SnO_2 NPs based on the influence of thermal calcination. The structural and optical analyses such as the crystallite size, full-width half maximum (FWHM), dislocation density, lattice distortion, functional group bonding, morphology, elemental composition, reflection property, and band gap value were investigated for attaining an optimal efficacy for the suitable applications.

2. Methodology

2.1. Preparation of SnO_2 NPs

The production of pure nanocrystalline SnO_2 NPs was carried out using a similar protocol described in the former literature [27-28].

2.2. Characterization

The morphological and elemental composition of SnO_2 NPs were studied using the FESEM brand JEOL model JSM-7600F. X-Ray analyses were carried out using PANalytical X'pert PRO using Cu Kα radiation (λ =1.17545Å) at ca. 2θ = 5º-90º with 45 kV and a scan speed of 0.417782*/sec with 40 mA. UV-visible analyses were performed using the Varian model Carry 5000 within 200 to 800 nm regions. FTIR-ATR analyses were performed using Perkin Elmer Spectrum 400 within the range of 400 to 4000 cm^{-1}.

3. Results and Discussions

3.1. XRD analysis

The XRD patterns displayed in **Figure 1** designated the development of single-rutile of SnO_2 NPs, in accordance with the JCPDS card no.01-077-0452. The peaks at 2q values of 26.9º, 34.1º, 38.2º, 51.1˚, 55.0˚, 58.2˚, 62.2˚, 65.3˚, 66.3˚, 71.6˚, 78.9˚, and 84.0˚ can be indexed as (110), (101), (200), (211), (220), (002), (310), (112), (301), (202), (321) and (222) planes, in agreement to previous literature and no peaks relating to any alien phases were detected [29-30]. The correlation between thermal calcination at 300 to 900ºC with the peak intensity, altitude, and narrowness was observed. Moreover, the number of diffraction peaks increases with the rising of the thermal temperature. The introduction of thermal energy at 300ºC to 500ºC is deficient for transforming the amorphous to the crystallinity phase giving a low intensity peak. Besides, the disorder arrangement of atoms in the planes also caused this condition, leading to incomplete nucleation [31]. As a result, the three prominent peaks having sharpness patterns represented by (110), (101), and (211) planes were broadened, thus suggesting the favored temperature to be 600ºC to 900ºC. At these higher temperatures, the necessary energy was fully occupied to facilitate the electron diffusion in calcination process to complete the full degree for construction of crystalline SnO_2 NPs, incrementing the crystallite size [32]. Besides, the arrangement of the well-ordered atoms in the crystal surfaces and grain interfaces also contributes to the high intensity of the diffraction peaks and decrease in the FWHM. The analysis of the crystallinity size (D) of SnO_2 NPs was carried out by using Scherrer's formula as shown in equation 1, where λ is the X-ray wavelength of Cu Kα (1.54 Å), θ is Bragg's diffraction angle, β is the full width at the half maximum in radians, and k is the unknown shape factor [33]:

$$D = \frac{k\lambda}{\beta \, Cos\theta} \qquad (1)$$

Table 1 displays the XRD analysis of calcined samples within the thermal temperature of 300ºC to 900ºC, indicating the parameters involved in the transformation of the amorphous to tetragonal rutile crystalline structure of SnO_2 NPs. The parameters at (110) plane orientations are measured as it has a high atomic density in SnO_2 NPs, and the interplanar distance or d-spacing (d) of unit cell parameters a and c were calculated with the help of equation 2 [34-36].

$$\frac{1}{d^2} = \frac{(h^2+k^2)}{a^2+\frac{l^2}{c^2}} \qquad (2)$$

The increase of the temperature directs lower value of FWHM was attributed to the change of the arrange tropism of the cells in the ultrafine powder, particularly to the orderless array of atoms in the crystal surfaces and grain interfaces (**Figure 2**) [37].

At this point, the introduction of higher calcination temperature promotes the growth of crystallinity, thus increasing the size of nanoparticles. A slow increase of crystallite size in the early stage of calcination from 300ºC to 500ºC is probably due to the presence of water molecules that prevent the rapid growth of crystal (**Figure 3**) [38]. Later, with sufficient energy, the diffusion of atoms from the grain boundary to the grain section occurred, making an increment in the crystallite size [39]. With the contribution of heating temperature, the cell volume is reduced, and the number of unit cells is boosted, as indicated by the values calculated using equation 3 [38,40].

$$n = \frac{\pi D^3}{6V} \quad (3)$$

Dislocation density, related to the number of defects in the grown nano-crystalline powder was found to be reduced by the increment of calcination temperature, which leads to increase of the crystal growth and decreasing the defects in crystallites, with the rapid decrement from 300ºC to 500ºC (**Figure 4**) [38]. Through systematic increments of temperatures, the particle size increases with a consistent decrease in the proportion of the surface atoms, thus leading to a decrease in defect concentration and reducing the crystal lattice distortion [37,40]. The value of the dislocation density (δ) and lattice distortion (n) are calculated using the equation 4 and 5 as follows [41]:

$$\delta = \frac{1}{D^2} \quad (4)$$

$$\sqrt{\varepsilon^2} = \frac{1}{D}\frac{1}{sin\theta}\frac{\pi}{\lambda}\sqrt{\frac{\pi^2 k^2 - 4}{32}} \quad (5)$$

3.2. FTIR analysis

The structural evidence for SnO_2 NPs construction was further confirmed by FTIR analysis (**Figure 5**). The pertinent function, as evidenced by the absorption band at 606 $cm^{-1,}$ is attributed to the Sn-O-Sn group. Besides, the confirmation was also strengthened by the absorption peak around 1112 cm^{-1} [42-43]. The absorption bands obtained are equal for all temperatures applied, suggesting that the temperature variation does not affect the absorption value of respective bondings. By having these proofs, the formation of SnO_2 NPs was confirmed, and the XRD results suggested for the crystalline phase were validated.

3.3. FESEM and EDX analysis

The morphological images of SnO_2 NPs in **Figure 6** indicate a formation corresponding to a spherical and uniform distribution. This is well supported by former literature described by Dheyab et al., in which the greenly synthesized SnO_2 NPs mostly obtained in spherical or quasi/semi-quasi nanoparticles [44]. A very tinny nanoscale particle was obtained from SnO_2 NPs calcined at 600ºC, making it unlikely to be measured. Eventually, SnO_2 NPs prepared at 700ºC were estimated at 18 nm, and as the temperatures rose, the size gradually increased to give 26 nm and 28 nm nanoscale sizes for SnO_2 NPs calcined at 800ºC and 900ºC, respectively. This systematic progression is evident in the XRD analysis regarding the results of crystallite size. From the EDX analysis, the rise in calcination temperature has led to the suppression of chloride ions, leaving only pure Sn and O elements (**Figure 7**). The Sn atom was found to be a significant contributor to weight percentages in all temperatures (**Table 2**).

3.4. UV-vis diffuse reflectance (UV-DRS) analysis and band gap

The optical characteristic of SnO_2 NPs was further studied under UV-Vis DRS analysis, and the spectrum is displayed in **Figure 8**. The absorption edge relates to electron transitions from the valence band to the conduction band, and this edge can be applied to compute the band gap values [45]. The reflectance value presumably resulted from harboring light scattering and later promoting light harvesting [46]. About 86 % of reflectance value was gained from SnO_2 NPs prepared at 600ºC, while approximately 80 % for the latter. Then, the reflectance values were translated to the band gaps using the Kubelka-Munk equation 6, where F(R) is the Kubelka-Munk functions, and k, s represents the K-M scattering and absorption coefficients [47-49].

$$F(R) = \frac{(1-R)^2}{2R} = \frac{k}{s} \quad (6)$$

Figure 8 shows the plot of the energy of the optical bandgap at different calcination temperatures. The direct bandgap energy values were obtained from the intercepts with the energy axis. The values obtained are 4.75 eV, 4.86 eV, 4.89 eV, and 4.90 eV for 600ºC, 700ºC, 800ºC, and 900ºC, respectively. From the former reports, the change in band gap value is related to the crystallite size of nanoparticles. **Figure 9** demonstrated a blue shift as the temperature increases in the calcination process owing to the decreases in crystallite size. The size of the crystal is reduced, and the band gap increases, resulting in the shift of the absorption edge to the greater energy. Besides, quantum confinement might also be one of the causes of the shift [50-51].

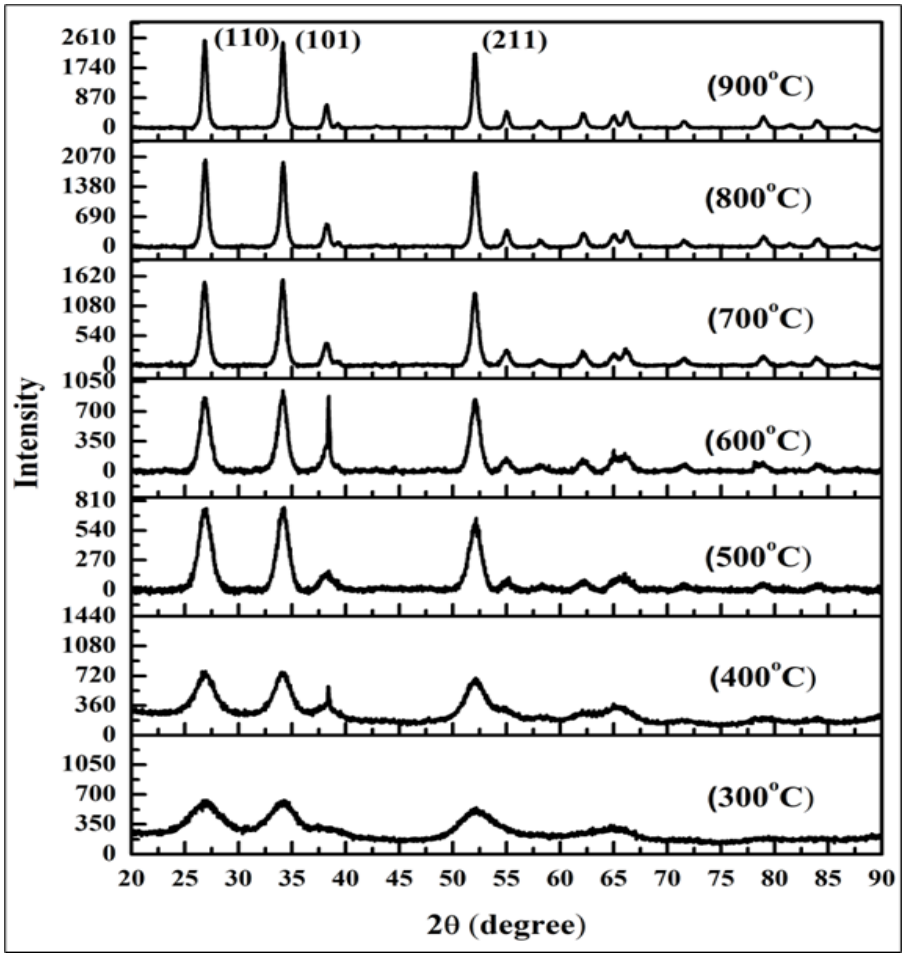

Fig. 1. The diffraction peaks of XRD of SnO_2 NPs at different thermal calcination temperatures.

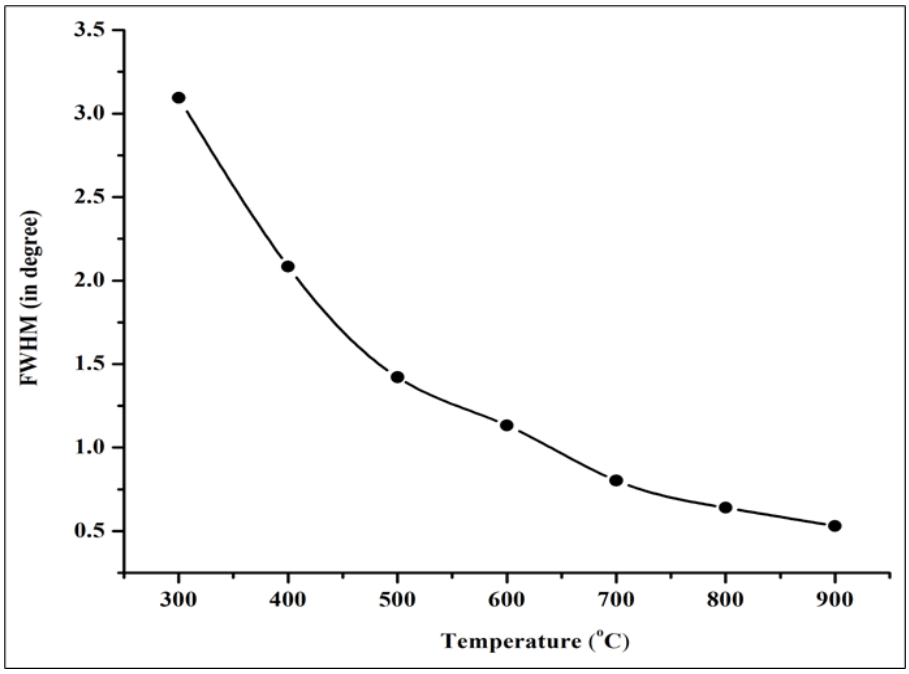

Fig. 2. Dependency of the FWHM of the (110) plane on the calcination temperatures.

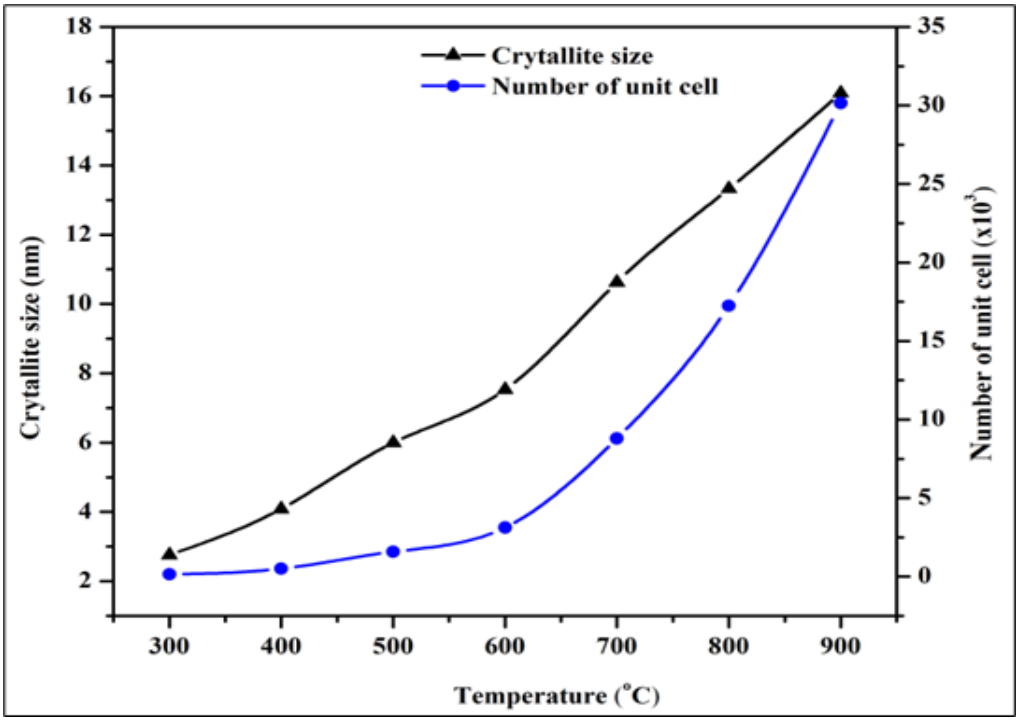

Fig. 3. Dependency of the crystallite size and number of unit cell planes on the calcination temperatures.

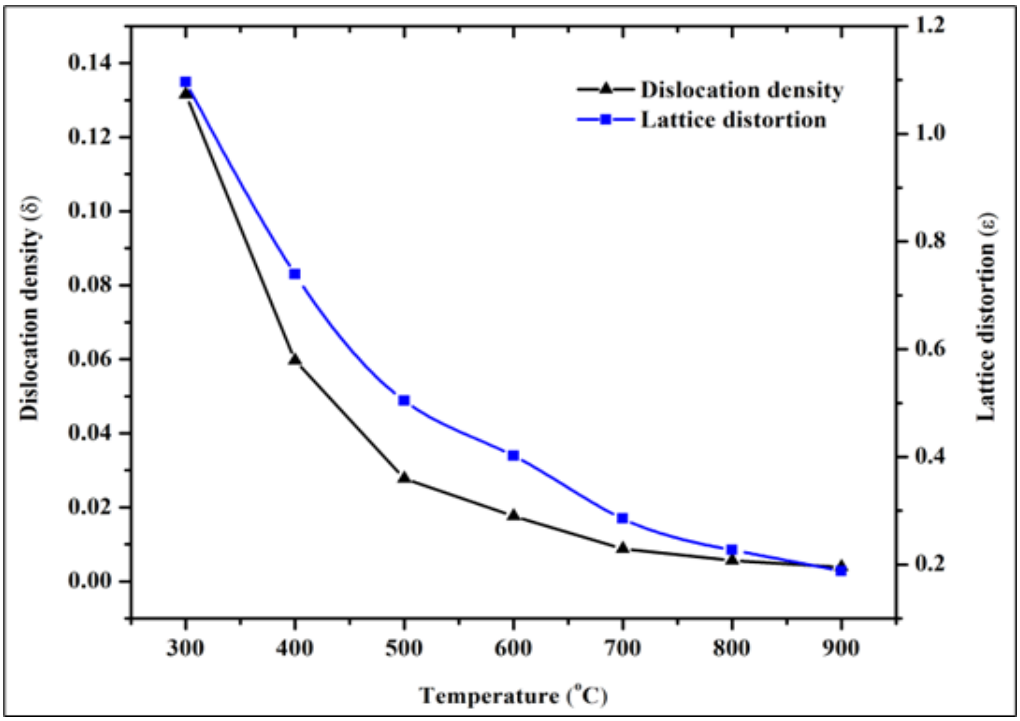

Fig. 4. Variation of dislocation density and lattice distortion as a function of temperatures.

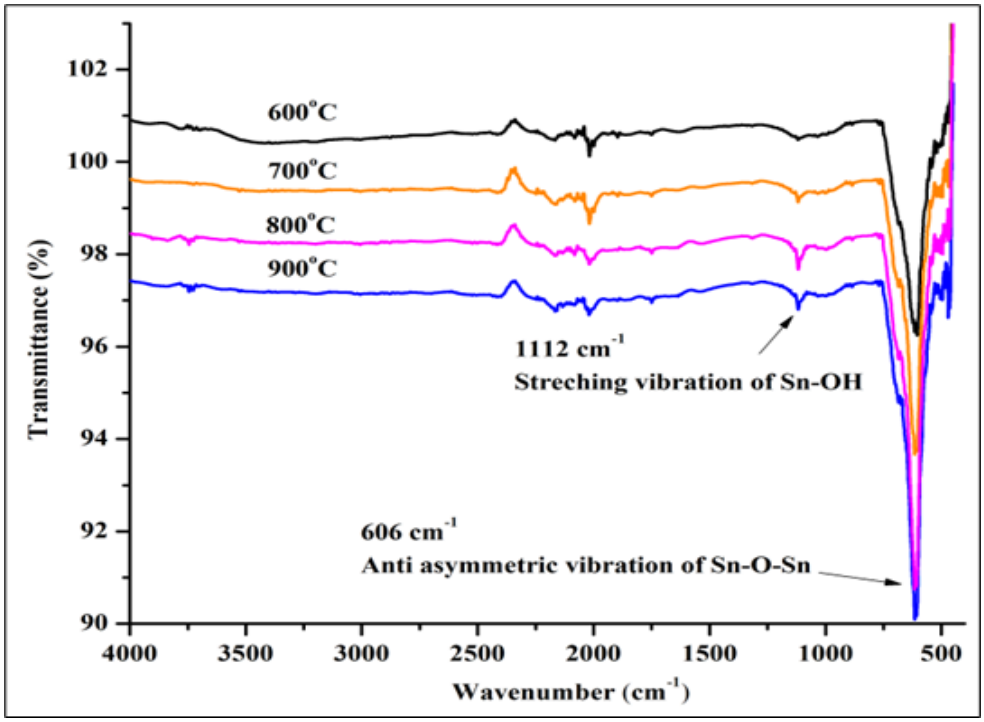

Fig. 5. FTIR spectra of SnO_2 NPs.

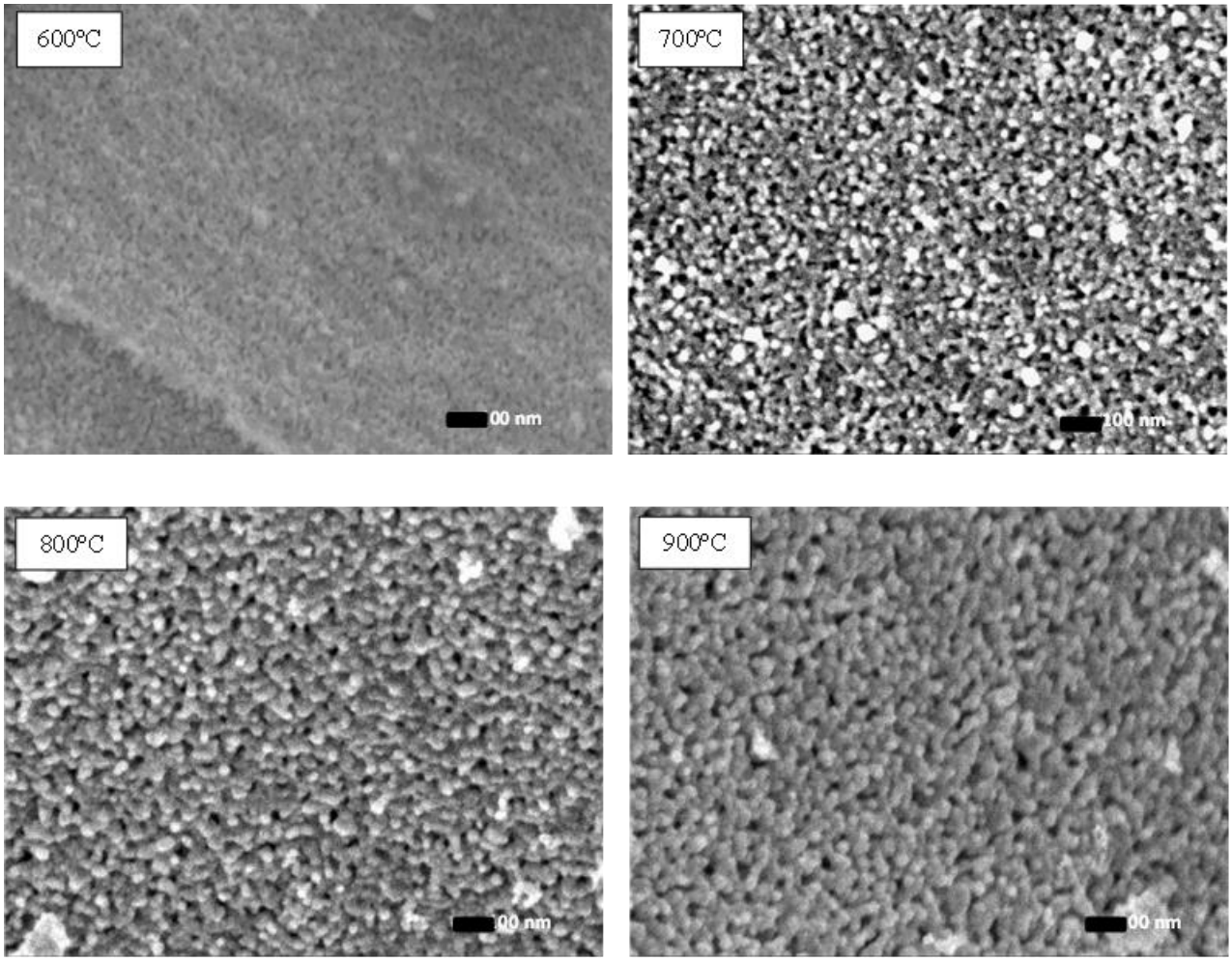

Fig. 6. FESEM images of SnO_2 NPs calcined at 600ºC to 900ºC.

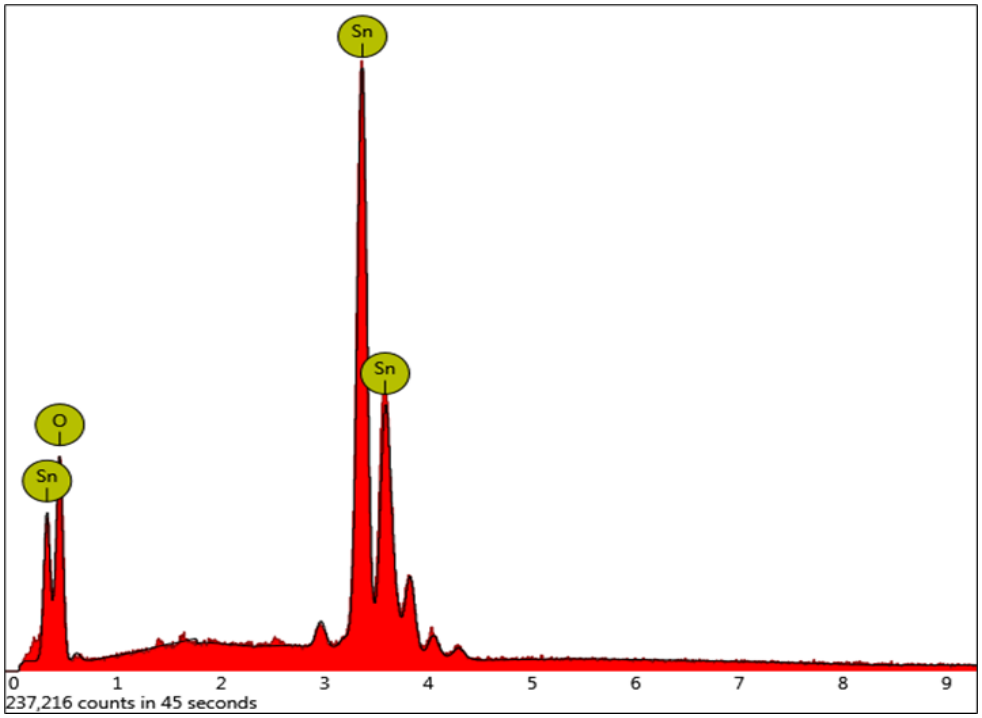

Fig. 7. EDX spectrum for SnO_2 NPs calcined at 900°C.

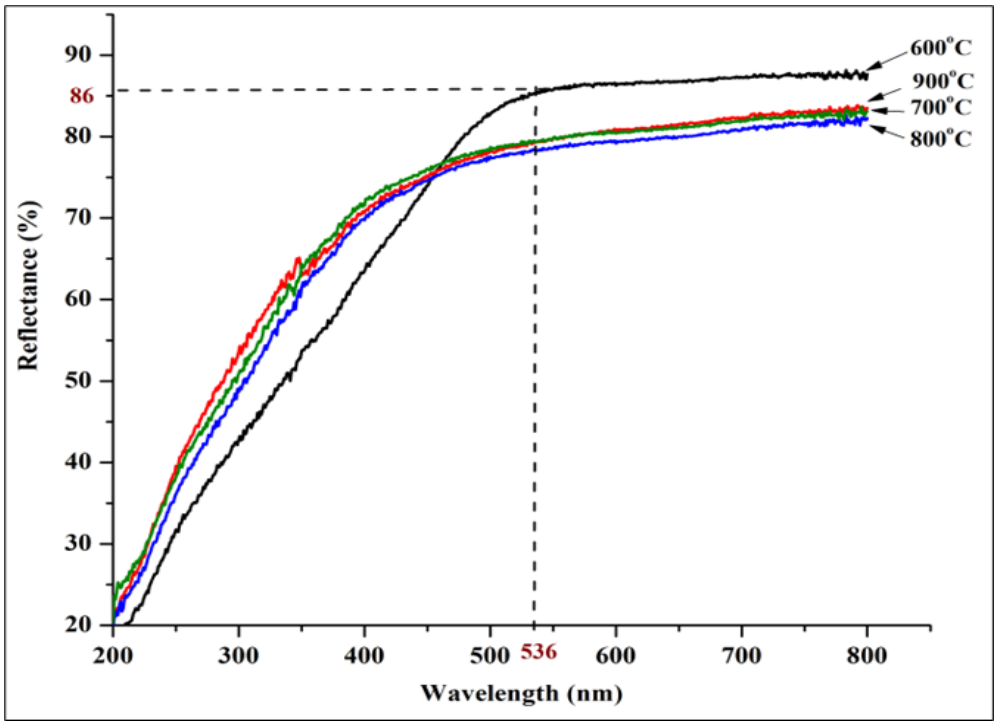

Fig. 8. UV-DRS of SnO_2 NPs calcined at 600°C to 900°C.

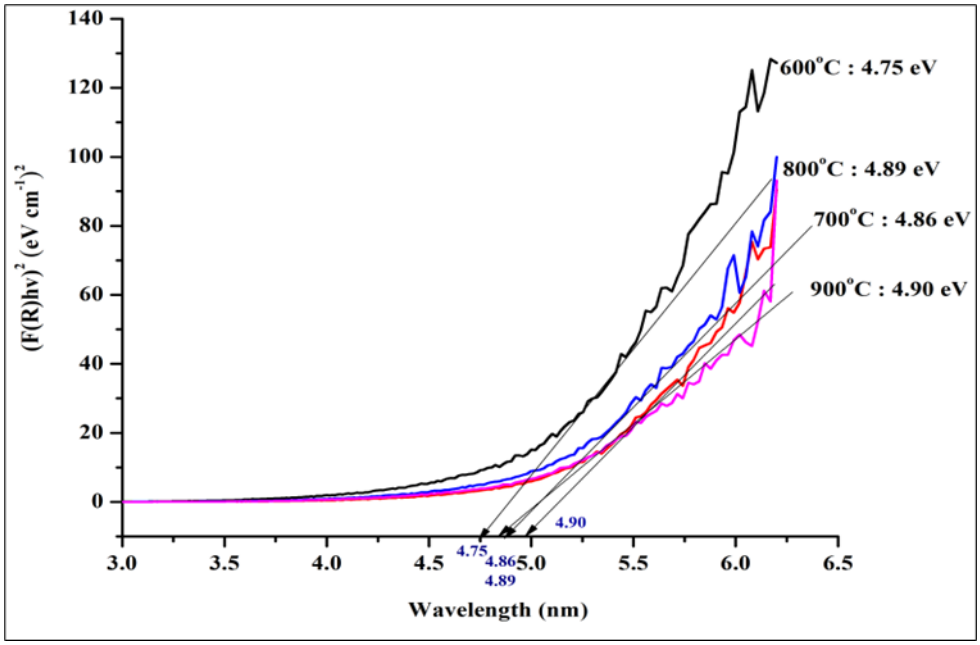

Fig. 9. Band gap plot of SnO_2 NPs calcined at 600°C to 900°C.

Table 1: The parameters measured for pure nanocrystalline of SnO_2 NPs.

Temp. (°C)	D (nm)	d-spacing (nm)	FWHM (°)	Lattice constant (Å)		Unit volume (Å³)	Number of unit cell (n)	Dislocation Density (δ)	Lattice distortion (ε)
				a=b	c				
300	2.76	0.3301	3.094	4.73	3.18	71.47	0.15	0.132	1.09
400	4.09	0.3724	2.083	4.73	3.18	71.47	0.50	0.059	0.74
500	6.00	0.2620	1.421	4.73	3.18	71.39	1.58	0.027	0.50
600	7.53	0.1742	1.132	4.74	3.19	71.74	3.11	0.017	0.40
700	10.63	0.3306	0.802	4.73	3.18	71.57	8.79	0.009	0.29
800	13.33	0.2623	0.640	4.74	3.19	71.91	17.23	0.006	0.23
900	16.09	0.1753	0.530	4.75	3.19	72.34	30.14	0.004	0.19

Table 2: The weight and atomic percentages of SnO_2 NPs.

Calcinations temperature (°C)	Sn element		O element	
	Weight (%)	Atomic (%)	Weight (%)	Atomic (%)
600	63.84	19.01	34.69	76.65
700	64.18	19.45	35.82	80.55
800	64.34	19.56	35.66	80.44
900	62.75	18.51	37.25	81.49

4. Conclusions

Spherical SnO_2 NPs were synthesized by the green-synthesis method route, using *Pandanus amaryllifolius* leaves extract and tin chloride pentahydrate in a water medium. The SnO_2 NPs crystallized in a tetragonal rutile structure of (110) favored orientation. The calcining temperature predominantly influenced the crystallite size, dislocation density, lattice distortion, morphology, and band gap values. The crystallite size followed the calcining temperature by decreasing the dislocation density and lattice distortion. Besides, the contribution of heat signified the morphological progression from tiny to larger spherical. The result of optical analysis obtained band gap values between 4.75 eV to 4.90 eV, indicating that the absorption edge was blue and shifted as the temperature increased. The further development of these SnO_2 NPs is suggested to be used in the photocatalytic application.

References

[1] G. A. Mansoori, & T. F. Soelaiman. (2005). Nanotechnology--An introduction for the standards community. ASTM International.

[2] Y. T. Gebreslassie, & H. G. Gebretnsae, (2021). Green and cost-effective synthesis of tin oxide nanoparticles: a review on the synthesis methodologies, mechanism of formation, and their potential applications. Nanoscale research letters. 16 (1): 97.

[3] S. Bayda, M. Adeel, T. Tuccinardi, M. Cordani, & F. Rizzolio. (2019). The history of nanoscience and nanotechnology: from chemical–physical applications to nanomedicine. Molecules. 25 (1): 112.

[4] L. E. Ahmadabad, F. S. Kalantari, H. Liu, A. Hasan, N. A. Gamasaee, Z. Edis, ... & Y. Cai. (2021). Hydrothermal method-based synthesized tin oxide nanoparticles: Albumin binding and antiproliferative activity against K562 cells. Materials Science and Engineering: C. 119: 111649.

[5] F. Zoller, D. Böhm, T. Bein, & D. Fattakhova-Rohlfing. (2019). Tin oxidebased nanomaterials and their application as anodes in lithium-ion batteries and beyond. ChemSusChem. 12 (18): 4140-4159.

[6] J. Saddique, H. Shen, Ge, J., Huo, X., Rahman, N., Mushtaq, M., ... & Al-Shehri, H. (2022). Synthesis and Characterization of $Sn/SnO_2/C$ Nano-Composite Structure: High-Performance Negative Electrode for Lithium-Ion Batteries. Materials. 15 (7): 2475.

[7] G. K. Dalapati, H. Sharma, A. Guchhait, N. Chakrabarty, P. Bamola, Q. Liu, ... & M. Sharma. (2021). Tin oxide for optoelectronic, photovoltaic and energy storage devices: a review. Journal of materials chemistry A. 9 (31): 16621-16684.

[8] J. A. Smith, O. S. Game, J. E. Bishop, E. L. Spooner, R. C. Kilbride, C. Greenland, ... & D. G. Lidzey. (2020). Rapid scalable processing of tin oxide transport layers for perovskite solar cells. ACS Applied Energy Materials. 3 (6): 5552-5562.

[9] J. H. Lee, Y. J. You, M. A. Saeed, S. H. Kim, S. H. Choi, S. Kim, ... & J. W. Shim. (2021). Undoped tin dioxide transparent electrodes for efficient and cost-effective indoor organic photovoltaics (SnO_2 electrode for indoor organic photovoltaics). NPG Asia Materials. 13:(1), 43.

[10] M. Chen, X. Chen, W. Ma, X. Sun, L. Wu, X. Lin, ... & S. Chen. (2022). Highly stable SnO_2-based quantum-dot light-emitting diodes with the conventional device structure. ACS nano. 16 (6): 9631-9639.

[11] Y. Masuda. (2022). Recent advances in SnO_2 nanostructure based gas sensors. Sensors and Actuators B: Chemical. 364: 131876.

[12] Z. Kang, D. Zhang, T. Li, X. Liu, & X. Song. (2021). Polydopamine-modified SnO_2 nanofiber composite coated QCM gas sensor for high-performance formaldehyde sensing. Sensors and Actuators B: Chemical. 345: 130299.

[13] E. M. Bakhsh, K. Akhtar, T. M. Fagieh, S. B. Khan, & A. M. Asiri. (2021). Development of alginate@ tin oxide–cobalt oxide nanocomposite based catalyst for the treatment of wastewater. International Journal of Biological Macromolecules. 187: 386-398.

[14] I. Buniyamin, R. M. Akhir, N. A. Asli, Z. Khusaimi, M. F. Malek, & M. R. Mahmood. (2022). Nanotechnology applications in biomedical systems. Current Nanomaterials. 7 (3): 167-180.

[15] D. Mohanta, & M. Ahmaruzzaman. (2016). Tin oxide nanostructured materials: an overview of recent developments in synthesis, modifications and potential applications. RSC advances. 6 (112): 110996-111015.

[16] W. Ahmad, A. Pandey, V. Rajput, V. Kumar, M. Verma, & H. Kim. (2021). Plant extract mediated cost-effective tin oxide nanoparticles: a review on synthesis, properties, and potential applications. Current Research in Green and Sustainable Chemistry. 4: 100211.

[17] H. J. Kim, J. H. Son, & D. S. Bae. (2011). Synthesis and characterization of SnO_2 nanoparticles by hydrothermal processing. Kor. J. Mater. Res. 21 (8): 415-418.

[18] D. Murzalinov, E. Dmitriyeva, I. Lebedev, E. A. Bondar, A. I. Fedosimova, & A. Kemelbekova. (2022). The Effect of pH Solution in the Sol-Gel Process on the Structure and Properties of Thin SnO_2 Films. Processes. 10 (6): 1116.

[19] M. J. Alegbe, B. A. Moronkola, A. O. Elesho, O. S. Ayanda, & L. F. Petrik. (2022). Physicochemical Characterization of Tin Oxide Synthesized from Acid Mine Drainage Using Tin II Chloride. American Journal of Chemistry. 12 (1): 10-17.

[20] L. C. Nehru, & C. Sanjeeviraja. (2014). Rapid synthesis of nanocrystalline SnO_2 by a microwave-assisted combustion method. Journal of Advanced Ceramics. 3: 171-176.

[21] P. Kumar, & S. M. Dharmaprakash. (2022). Influence of substrate temperature and laser wavelength on the structural, optical and electrical properties of laser ablated tin oxide thin films. In IOP Conference Series: Materials Science and

Engineering (Vol. 1221, No. 1, p. 012023). IOP Publishing.

[22] G. E. Patil, D. D. Kajale, D. N. Chavan, N. K. Pawar, P. T. Ahire, S. D. Shinde, ... & G. H. Jain. (2011). Synthesis, characterization and gas sensing performance of SnO_2 thin films prepared by spray pyrolysis. Bulletin of Materials Science. 34: 1-9.

[23] S. Gorai. (2018). Bio-based synthesis and applications of SnO_2 nanoparticles-an overview. Journal of Materials and Environmental Science. 9 (10).

[24] S. Matussin, M. H. Harunsani, A. L. Tan, & M. M. Khan. (2020). Plant-extract-mediated SnO_2 nanoparticles: synthesis and applications. ACS Sustainable Chemistry & Engineering. 8 (8): 3040-3054.

[25] N. Thatsanasuwan, W. Srichamnon, C. Chupeerach, W. Kriengsinyos, & U. Suttisansanee. (2015). Antioxidant activities of Pandanus amaryllifolius leaves extracted under four designed extraction condition. Food and Applied Bioscience Journal. 3: 130-136.

[26] M. M. Zakaria, U. H. Zaidan, S. Shamsi, & S. S. A. Gani. (2020). Chemical composition of essential oils from leaf extract of pandan, Pandanus amaryllifolius ROXB. Malaysian Journal of Analytical Sciences. 24 (1): 87-96.

[27] I. Buniyamin, R. M. Akhir, N. A. Asli, Z. Khusaimi, & M. R. Mahmood. (2021). Effect of calcination time on biosynthesised SnO_2 nanoparticles using bioactive compound from leaves extract of Chromolaena Odorata. In AIP Conference Proceedings (Vol. 2368, No. 1). AIP Publishing.

[28] P. Oungkanitanon, S. Cheunkar, W. Liewrian, & P. Asanithi. (2021). Serine/Graphene Oxide modified Electrode for Electrochemical Determination of Uric acid. In Proceeding of 5th International Symposium on Advanced Materials and Nanotechnology (p. 18).

[29] I. Buniyamin, R. M. Akhir, N. A. Asli, Z. Khusaimi, & M. R. Mahmood. (2021). Biosynthesis of SnO_2 nanoparticles by aqueous leaves extract of Aquilaria malaccensis (agarwood). In IOP Conference Series: Materials Science and Engineering (Vol. 1092, No. 1, p. 012070). IOP Publishing.

[30] M. Kumar, A. Mehta, A. Mishra, J. Singh, M. Rawat, & S. Basu. (2018). Biosynthesis of tin oxide nanoparticles using Psidium Guajava leave extract for photocatalytic dye degradation under sunlight. Materials Letters. 215: 121-124.

[31] P. Khaenamkaew, D. Manop, C. Tanghengjaroen, & W. Palakawong Na Ayuthaya. (2020). Crystal structure, lattice strain, morphology, and electrical properties of SnO_2 nanoparticles induced by low calcination temperature. Advances in Materials Science and Engineering. 1-10.

[32] V. K. Vidhu, & D. Philip. (2015). Biogenic synthesis of SnO2 nanoparticles: evaluation of antibacterial and antioxidant activities. Spectrochimica Acta Part A: Molecular and Biomolecular Spectroscopy. 134: 372-379.

[33] T. T. Bhosale, H. M. Shinde, N. L. Gavade, S. B. Babar, V. V. Gawade, S. R. Sabale, R. J. Kamble, B. S. Shirke, & K. M. Garadkar. (2018). Biosynthesis of SnO_2 nanoparticles by aqueous leaf extract of Calotropis gigantea for photocatalytic applications. Journal of materials science and materials in electronics. 1-10.

[34] J. T. Wang, X. L. Shi, W. W. Liu, X. H. Zhong, J. N. Wang, L. Pyrah, ... & K. Tsuri. (2014). Influence of preferred orientation on the electrical conductivity of fluorine-doped tin oxide films. Scientific reports. 4 (1): 3679.

[35] H. Köse, Ş. Karaal, A. O. Aydin, & H. Akbulut. (2015). Structural properties of size-controlled SnO_2 nanopowders produced by sol–gel method. Materials Science in Semiconductor Processing. 38: 404-412.

[36] A. Ayeshamariam. (2013). Synthesis, structural and optical characterizations of SnO_2 nanoparticles. Journal of Photonics Spintron. 2: 4-8.

[37] S. Gao, L. Pang, H. Che, & X. Zhou. (2004). Synthesis of SnO_2 nanocrystals by solid state reaction followed by calcination. China Particuology. 2 (4): 177-181.

[38] A. Gaber, M. A. Abdel- Rahim, A. Y. Abdel-Latief, M. N. Abdel-Salam. (2014). Influence of calcination temperature on the structure and porosity of nanocrystalline SnO_2 synthesized by a conventional precipitation method. International journal of electrochemical science. 9: 81-95.

[39] M. P. Subramaniam, G. Arunachalam, R. Kandasamy, P. Veluswam, & I. Hiroya. (2018). Nanoparticles prepared by sol-gel method Effect of pH and annealing temperature on the properties of tin oxide nanoparticles prepared by sol-gel method. Journal of Materials Science Materials in Electronics. 29: 1-10.

[40] L. C. Nehru. (2014). Preparation and characterization of nanosize SnO_2 nanopowders by precipitation method. International journal of applied nanotechnology. 1: 1-12.

[41] N. Rani, & N. Jaggi. (2020). Effect of reaction temperature on the structural and electronic properties of stannic oxide nanostructures. Bulletin of Materials Science. 43 (1): 146.

[42] E. Gomathi, M. Jayapriya, & M. Arulmozhi. (2021). Environmental benign synthesis of tin oxide (SnO_2) nanoparticles using Actinidia deliciosa (Kiwi) peel extract with enhanced catalytic properties. Inorganic Chemistry Communications. 130: 108670.

[43] K. C. Suresh, S. Surendhiran, P. M. Kumar, E. R. Kumar, Y. S. Khadar, & A. Balamurugan. (2020). Green synthesis of SnO_2 nanoparticles using Delonix elata leaf extract: Evaluation of its structural, optical, morphological and photocatalytic properties. SN Applied Sciences. 2: 1-13.

[44] M. A. Dheyab, A. A. Aziz, M. S. Jameel, & N. Oladzadabbasabadi. (2022). Recent advances in synthesis, modification, and potential application of tin oxide nanoparticles. Surfaces and Interfaces. 28, 101677.in synthesis, modification, and potential application of tin oxide nanoparticles. Surfaces and Interfaces. 28: 101677.

[45] A. Kar, J. Olszówka, S. Sain, S. R. I. Sloman, O. Montes, A. Fernández, ... & A. E. Wheatley. (2019).

Morphological effects on the photocatalytic properties of SnO_2 nanostructures. Journal of Alloys and Compounds. 810: 151718.

[46] D. Zhao, G. Sheng, C. Chen, & X. Wang. (2012). Enhanced photocatalytic degradation of methylene blue under visible irradiation on graphene@ TiO_2 dyade structure. Applied Catalysis B: Environmental. 111: 303-308.

[47] V. Senthilkumar, K. Senthil, & P. Vickraman. (2012). Microstructural, electrical and optical properties of indium tin oxide (ITO) nanoparticles synthesized by co-precipitation method. Materials Research Bulletin. 47 (4), 1051-1056.

[48] I. Buniyamin, R. M. Akhir, N. A. Asli, Z. Khusaimi, & M. Rusop. (2022). Green synthesis of tin oxide nanoparticles by using leaves extract of Chromolaena Odorata: the effect of different thermal calcination temperature to the energy band gap. Materials Today: Proceedings. 48: 1805-1809.

[49] I. Buniyamin, R. M. Akhir, M. Z. Nurfazianawatie, H. Omar, N. S. A. Malek, N. F. Rostan, ... & M. Rusop. (2023). Aquilaria malaccensis and Pandanus amaryllifolius mediated synthesis of tin oxide nanoparticles: The effect of the thermal calcination temperature. Materials Today: Proceedings. 75: 23-30.

[50] P. Chand. (2019). Effect of pH values on the structural, optical and electrical properties of SnO_2 nanostructures. Optik. 181: 768-778.

[51] A. G. Habte, F. G. Hone, & F. B. Dejene. (2020). Effect of solution pH on structural, optical and morphological properties of SnO_2 nanoparticles. Physica B: Condensed Matter. 580: 411832.